

THE MAGELLANIC QUASARS SURVEY. II. CONFIRMATION OF 144 NEW ACTIVE GALACTIC NUCLEI BEHIND THE SOUTHERN EDGE OF THE LARGE MAGELLANIC CLOUD

SZYMON KOZŁOWSKI¹, C. S. KOCHANEK^{2,3}, A. M. JACYSZYN¹, A. UDALSKI¹, M. K. SZYMAŃSKI¹, R. POLESKI¹, M. KUBIAK¹, I. SOSZYŃSKI¹, G. PIETRZYŃSKI^{1,4}, Ł. WYRZYKOWSKI^{1,5}, K. ULACZYK¹, AND P. PIETRUKOWICZ¹

Draft version March 9, 2018

ABSTRACT

We quadruple the number of quasars known behind the Large Magellanic Cloud (LMC) from 55 (42 in the LMC fields of the third phase of the Optical Gravitational Lensing Experiment (OGLE)) to 200 by spectroscopically confirming 169 (144 new) quasars from a sample of 845 observed candidates in four ~ 3 deg² Anglo-Australian Telescope/AAOmega fields south of the LMC center. The candidates were selected based on their *Spitzer* mid-infrared colors, X-ray emission, and/or optical variability properties in the database of the OGLE microlensing survey. The contaminating sources can be divided into 115 young stellar objects (YSOs), 17 planetary nebulae (PNe), 39 Be and 24 blue stars, 68 red stars, and 12 objects classed as either YSO/PN or blue star/YSO. There are also 402 targets with either featureless spectra or too low signal-to-noise ratio for source classification. Our quasar sample is 50% (30%) complete at $I = 18.6$ mag (19.3 mag). The newly discovered active galactic nuclei (AGNs) provide many additional reference points for proper motion studies of the LMC, and the sample includes 10 bright AGNs ($I < 18$ mag) potentially suitable for absorption line studies. Their primary use, however, is for detailed studies of quasar variability, as they all have long-term, high cadence, continuously growing light curves from the microlensing surveys of the LMC. Completing the existing Magellanic Quasars Survey fields in the LMC and Small Magellanic Cloud should yield a sample of ~ 700 well-monitored AGNs, and expanding it to the larger regions covered by the OGLE-IV survey should yield a sample of ~ 3600 AGNs.

Subject headings: galaxies: active – Magellanic Clouds – quasars: general

1. INTRODUCTION

Kelly et al. (2009), Kozłowski et al. (2010a), and MacLeod et al. (2010) introduced, developed, and applied a new approach to quantitatively modeling the variability of individual quasars, describing the light curves as damped random walks (DRW) characterized by two parameters, a timescale and an amplitude. These parameters are then found to be correlated with the physical properties of the quasar – wavelength, luminosity, and black hole mass. Unfortunately, accurately measuring the parameters of individual quasars requires long (\gtrsim decade) well-sampled light curves that are generally not available (see MacLeod et al. 2011). While this may ultimately be solved by projects such as the Panoramic Survey Telescope and Rapid Response System (PanSTARRS; Kaiser et al. 2002) and the Large Synoptic Survey Telescope (LSST; Ivezić et al. 2008), their cadences are not ideal and it still requires a decade of operations to accumulate the light curves. This makes it challenging to expand on this promising new approach to probing quasar physics.

There are, however, quasars⁶ with almost two decades

of well-sampled light curves – the quasars lying in the regions surveyed by microlensing projects such as the Optical Gravitational Lensing Experiment⁷ (OGLE; e.g., Udalski et al. 2008a), MACHO (e.g., Alcock et al. 2000), and the Microlensing Observations in Astrophysics (MOA; e.g., Noda et al. 2002). For example, the combined phases of the OGLE survey (OGLE-II to OGLE-IV) span 15 years with up to 1000 epochs in I -band and a few dozen in V -band for approximately 40 million sources with $I < 21$ mag in the Magellanic Clouds, and the light curves continue to be extended by the OGLE-IV survey.

The challenge is identifying the rare quasars in these dense stellar fields. A combination of serendipity (e.g., Schmidtke et al. 1994; Clocchiatti et al. 2003), X-ray (Crampton et al. 1997; Dobrzycki et al. 2002, 2003b), and crude variability measures (Dobrzycki et al. 2003a; Geha et al. 2003; Dobrzycki et al. 2005) had succeeded in identifying only 55 and 28 quasars in the LMC and SMC, respectively, as of 2010. In Kozłowski & Kochanek (2009), we showed that the mid-IR selection techniques developed for extragalactic surveys (Stern et al. 2005) could also be applied to dense stellar regions, albeit with some contamination from the relatively rare dusty stars (e.g., young stellar objects (YSOs), planetary nebulae (PNe), etc.). In Kozłowski et al. (2010a), we showed that the DRW variability parameters of quasars differed from those of variable stars, providing a more quantitative approach to variability-selecting quasars that has been expanded on in MacLeod et al. (2011) and Butler & Bloom

throughout this paper.

⁷ <http://ogle.astrouw.edu.pl/>

¹ Warsaw University Observatory, Al. Ujazdowskie 4, 00-478 Warszawa, Poland; e-mail: simkoz@astrouw.edu.pl

² Department of Astronomy, The Ohio State University, 140 West 18th Avenue, Columbus, OH 43210, USA

³ The Center for Cosmology and Astroparticle Physics, The Ohio State University, 191 West Woodruff Avenue, Columbus, OH 43210, USA

⁴ Departamento de Física, Universidad de Concepción, Casilla 160-C, Concepción, Chile

⁵ Institute of Astronomy, University of Cambridge, Madingley Road, Cambridge CB3 0HA, UK

⁶ Quasars, AGNs and QSOs will be used interchangeably

(2011). In a single test observation under poor conditions, Kozłowski et al. (2011) doubled the number of known quasars behind the SMC from 28 to 57.

Apart from studying variability, quasars in these fields are important tools for deriving more precise proper motions of the LMC, SMC and, potentially, the Galactic Bulge using the *Hubble Space Telescope (HST)* or, in the future, the *James Webb Space Telescope (JWST)*. Kallivayalil et al. (2006) and Piatek et al. (2008) based their LMC proper motions on 21 quasars. Further improvements require better measuring the internal motions of the Clouds, and this requires larger numbers of quasars well-distributed over the LMC disk. Based on Piatek et al. (2008), the newly confirmed LMC quasars we discuss here could be used to reduce the proper motion uncertainties by a factor of three, since our new quasars are distributed over a large $6 \times 4 \text{ deg}^2$ area of the LMC disk. We will also identify any bright quasars suitable for absorption studies of the LMC’s interstellar medium (ISM), as we expect 1, 10, and 74 quasars brighter than $I < 17, 18,$ and 19 mag in the four observed fields.

The goal of our Magellanic Quasars Survey (MQS) is to identify and characterize all these quasars, where we estimate a final sample of roughly 700 quasars in a complete survey of the OGLE-III project regions. Spectroscopy is essential not only for confirmation of the candidates but also to determine the luminosity, rest-wavelength and black hole masses (through the emission line widths) of the quasars, so that the variability parameters can be related to other physical properties. Relatively large numbers of quasars will be needed to explore this (minimally) three dimensional parameter space quantitatively. While the sample will be smaller than the ~ 9000 quasars we considered in MacLeod et al. (2010), the longer, more densely sampled light curves should let us examine the physical correlations with less “blurring” from the noisy parameter estimates obtained from the sparsely sampled Sloan Digital Sky Survey (SDSS) light curves, making it far easier to determine the intrinsic parameter distributions. In this paper, we report our preliminary results for the LMC, sadly reduced in scope by hurricane Yasi. In Section 2, we describe the selection methods leading to a sample of 2434 quasar candidates behind LMC. Section 3 describes the observation plan, the observations, and the data analysis. Section 4 introduces the new quasars and Section 5 discusses the contaminating sources. We discuss the results in Section 6 and summarize the paper in Section 7.

2. AGN CANDIDATE SELECTION

We selected targets based on their mid-IR, X-ray and/or photometric variability characteristics and we describe each method in detail below. The observations were designed for AAOmega, a 400-fiber spectrograph mounted on the 3.9 m Anglo-Australian Telescope (AAT; Sharp et al. 2006). The AAOmega instrument has many more fibers than the expected number of quasars in its field of view, so we kept candidates satisfying any of the selection criteria, thereby aiming for higher completeness at the price of higher contamination. There is no point in having empty fibers even if it means observing more contaminating stars.

2.1. Mid-IR-selected AGN Candidates

Stern et al. (2005) showed that active galactic nuclei (AGNs) have redder mid-IR colors than galaxies and stars, and that they form a distinctive group in the mid-IR color-color plane (see Lacy et al. 2004 and Eisenhardt et al. 2004, and also Assef et al. 2010, Gorjian et al. 2008, and Kozłowski et al. 2010b for the mid-IR colors of X-ray and variability selected AGNs). The red mid-IR colors of a typical AGN are not due to dust emission, so mid-IR-selected AGNs are generally normal $z \gtrsim 1$ broad-line quasars (see Assef et al. 2010, Assef et al. 2011). There is also no significant tendency for them to be Type II quasars. This is particularly true with the addition of a magnitude limit for the optical spectroscopy, since at most redshifts the emission from the disk is required to render the source bright enough to be observed.

In Kozłowski & Kochanek (2009), we used this approach to identify quasars in the LMC and SMC from the *Spitzer/IRAC* four-band photometry (i.e., 3.6, 4.5, 5.8, and $8.0 \mu\text{m}$) of the Surveying the Agents of a Galaxy’s Evolution project (SAGE; Meixner et al. 2006). The 5000 AGN candidates were divided into several categories. First, all the objects must be located inside the “Stern AGN wedge” (Stern et al. 2005). The locus of cool blackbodies passes through the wedge so the quasar sample is divided into group “A” if they are far from the blackbody locus, and “B” if they can be contaminated with cold stars. Second, the mid-IR color-magnitude diagram (CMD) was divided into regions heavily contaminated by YSOs and one that should principally contain quasars, based on mid-IR properties of YSOs from Whitney et al. (2008) and the mid-IR data from the 9 deg^2 of the Spitzer Deep Wide-Field Survey (SD-WFS; Ashby et al. 2009) of spectroscopically confirmed quasars from the AGN and Galaxy Evolution Survey (AGES; Kochanek et al. 2011). Finally, the candidates were classed as “a” if they had the optical-to-mid-IR colors of quasars in AGES and “b” if they did not.

The most interesting candidates are classed as QSO-Aa (quasar region, away from blackbody locus with QSO optical-to-mid-IR colors), but given the large number of AAOmega fibers, we targeted all classes of objects, excluding only those marked as “outside” (of the OGLE-III fields) or “faint” (not detected on the OGLE-III template images).

2.2. X-Ray-selected AGN Candidates

We searched for the OGLE-III counterparts to the 758 X-ray sources distributed over $10 \times 10 \text{ deg}^2$ of the LMC from Haberl & Pietsch (1999). The typical positional uncertainty for these X-ray sources is several arcseconds, so we cannot effectively target them without some additional selection criterion given the stellar densities. As a second criterion we chose the most optically variable source within 3σ of the X-ray position. In this case, variability simply means that the light curve is inconsistent with a constant flux, without any of the more quantitative variability selection criteria we discuss in the next section. This led to a sample of 205 X-ray candidates, of which 160 were also mid-IR-selected candidates and 99 satisfy the variability cuts presented in Section 2.3.

2.3. Variability-selected AGN Candidates

The OGLE-III database (Udalski et al. 2008a,b) contains the data for 9 years (2001–2009) of continuous monitoring ~ 35 million objects toward the LMC. We used this database to search for variable objects that are likely quasars based on the DRW model of their light curves (e.g., Kelly et al. 2009; Kozłowski et al. 2010a; MacLeod et al. 2010).

We prepared and analyzed the light curves as described in Kozłowski et al. (2010a). We use the timescale τ , scaled amplitude $\hat{\sigma}^2 = 2\sigma^2/\tau$, and the likelihood ratio $\ln L_{\text{best}}/\ln L_{\text{noise}}$ between the best fitting model and a white noise model corresponding to simply expanding the photometric errors. We also fit a power-law structure function (SF) and estimated its slope γ between 30 days and 2 years, and an amplitude A defined by the magnitude difference between the first and third quartile of the sorted light curve.

To remove unwanted variable sources, we use the following cuts: *Cut 1*. The average light curve magnitude is $I < 19.5$ mag; *Cut 2*. $\ln L_{\text{best}} > \ln L_{\text{noise}} + 2$; *Cut 3*. The SF slope $0.1 < \gamma < 0.9$ (e.g., see Schmidt et al. 2010); *Cut 4*. The I -band amplitude $A < 0.4$ mag (this removes large amplitude variable stars); MacLeod et al. (2010) report that some of ~ 9000 SDSS quasars occupy areas outside the τ - $\hat{\sigma}$ cut of Kozłowski et al. (2010a), therefore we decided to loosen the cut on the τ parameter and to ignore $\hat{\sigma}$ parameter, so *Cut 5* is $1 < \log(\tau) < 5$. When simply applied to the OGLE light curve database, this process yields $\sim 24,000$ candidates. The vast majority are due to two known systematic issues. First, bright variable stars typically generate several fake, fainter variable stars in their wings, and these “ghost” variables show long term irregular variability. Second, there can be small magnitude shifts between seasons, and (for one field in particular) the shifts were being misinterpreted as quasar-like variability. We carried out a quick visual inspection of all candidates, but this was over kill and would certainly be automated in any subsequent analysis. We were left with 1063 variability-selected candidates.

2.4. Final AGN Candidates Sample

The total number of candidates is 2434, distributed over ~ 30 deg² in the LMC. There are 2049 mid-IR-selected candidates and 385 non-mid-IR-selected candidates. Of the 2049 mid-IR (385 non-mid-IR) objects, 708 (355) are also variable and 160 (45) have associated X-ray emission. There are 1063 objects selected as variable, of which 708 are mid-IR sources, 99 are X-ray sources, and 84 both mid-IR and X-ray sources. Figure 1 shows how the samples overlap. Note that the limited overlap of the mid-IR and X-ray-selected AGNs is also seen in the spectroscopically confirmed samples of AGNs in the NDWFS field (e.g., Assef et al. 2011). The AAOmega fiber allocation software allows to prioritize targets from 1 (the lowest priority) to 9. We gave priorities of 9, 8, and 7 to sources selected by all three methods (84 sources), sources selected by only two methods (715 sources), and sources selected by only one method (1635), respectively.

3. DATA PREPARATION AND OBSERVATIONS

We are mostly interested in quasars located in the overlapping areas of the SAGE and OGLE-III surveys.

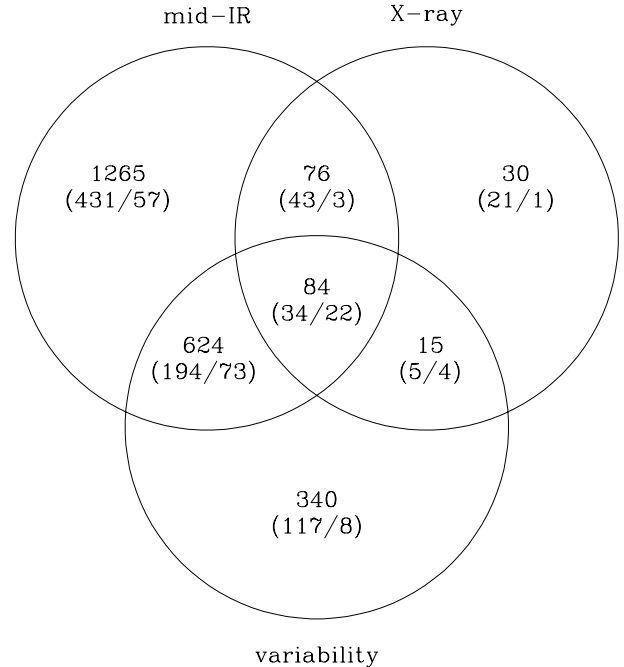


Figure 1. Venn diagram for all 2434 LMC MQS quasar candidates. The upper numbers give the number of candidates in each selection region. Priority 9 is given to AGN candidates located in the three overlapping circles (84 objects), priority 8 to objects in any two overlapping circles (715 objects), and priority 7 to sources in the non-overlapping areas (1635 objects). The lower numbers, in parenthesis, give the number of objects in the four observed fields followed by the number of spectroscopically confirmed AGN.

Table 1
The MQS LMC Fields, Number of Candidates, Number of Confirmed Quasars and Exposure Times.

Field	R.A.	Decl.	N_{cand}	N_{QSO}	T_{exp} (s)
LMC 01	04:41:43	-69:50:29	220
LMC 02	04:43:19	-68:19:18	197
LMC 03	04:56:52	-67:07:48	213
LMC 04	05:00:51	-70:27:49	221	41	1480
LMC 05	05:01:42	-68:49:26	269
LMC 06	05:14:27	-67:35:00	189
LMC 07	05:19:43	-69:31:07	307	36	5400
LMC 08	05:21:54	-71:02:48	247	60	3600
LMC 09	05:32:54	-68:31:01	230
LMC 10	05:41:31	-71:36:00	201	37	2550
LMC 11	05:41:56	-70:11:07	275
LMC 12	05:52:39	-68:57:51	183

Note. — Each field has a 1 deg radius. N_{QSO} does not have to add up to 144 new QSOs and 25 known QSOs, since the fields overlap slightly (see Figure 2) and one quasar can be observed in two or three fields.

We divided this LMC area into 12 fields (see Figure 2), each ~ 3 deg² and corresponding to the field of view of AAOmega. The basic information for each field is given in Table 1. The fields overlap slightly to avoid having gaps between them, so some of the quasar candidates were observed up to three times if they happened to fall into such an overlapping region. The total number of targeted objects in all 12 fields was 2678, of which several (less than 244) were targeted at least twice. On average there were 220 objects in a field, corresponding to ~ 70 sources deg⁻².

We observed the LMC fields on 2011 February 1–3. Unfortunately, due to arrival of tropical storm Yasi, we

were completely clouded out on the night of February 2 and partly on February 1 and 3. Of the 12 planned fields, we were able to execute only four (see Table 1 and Figure 2), and only one with the desired 1.5 hr (5400 s) exposure time. Nevertheless, the data are sufficient to confirm a large number of quasars. We observed 845 candidates of which we confirm 169 (144 new) in this paper. The yields divided by the AGN selection method are presented in Table 2.

We followed the spectral identification procedures from Paper I (Kozłowski et al. 2011). To find as many quasar emission lines in a spectrum as possible, we decided to use the widest available spectral coverage of $\sim 5100\text{\AA}$ (3750–8850 \AA) and a resolution of $R = 1300$. Each spectrum consists of a blue (580V) and a red (385R) channel that were spliced together at 5700 \AA . Some of the spectra appear to have a “wide broad line” around the splicing wavelength, mimicking the MgII (2800 \AA) line at a redshift of $z \approx 1.04$. We carefully checked all our $z \approx 1$ quasars for possible misidentifications. Our initial goal was to obtain three exposures of 1800 s per field, resulting in a median signal-to-noise ratio (S/N) of ~ 25 at $I = 19.5$ mag (calculated from obtained spectra). To subtract the sky flux contribution from each spectrum, we initially selected ~ 50 and finally used ~ 25 sky fibers, each positioned to avoid stellar emission based on the OGLE-III LMC catalogs (Udalski et al. 2008b). These catalogs were also used to find ~ 20 single and well separated bright guide stars for each field, of which 4–8 were used for guiding. The AAOmega FLD files were created with the CONFIGURE software, and the data reduction was performed using the 2DFDR software (Taylor et al. 1996).

As in Paper I, we searched each spectrum for the common (redshifted) quasar emission lines (e.g., Vanden Berk et al. 2001) Ly α at 1216 \AA , H δ at 4101 \AA , H γ at 4340 \AA , H β at 4861 \AA , H α at 6563 \AA , magnesium MgII at 2800 \AA , carbon CIV at 1549 \AA and CIII] at 1909 \AA , as well as the narrow forbidden lines of oxygen [O II] at 3727 \AA , [O III] at 4959 \AA or 5007 \AA . In general, we required the identification of two lines, except in the redshift range $0.7 < z < 1.2$, where we can only find MgII despite the broad spectral coverage.

4. NEW QUASARS

We identified 144 new quasars behind the LMC. Their basic parameters (including the identified lines) are presented in Table 3. We also confirmed the 25 known quasars that were in our target list (Table 4). Of these known quasars, we had flagged four only as probable quasars because their spectra were too noisy for reliable classification. We missed one known quasar, MQS J051140.7–710032.8, that had extremely low S/N in our data, although we verified its existence. These five sources are reported at the bottom of Table 4.

The newly discovered quasars cover the range of redshifts $z = 0.15$ –3.35 as shown in Figure 3. The deficit at $z \approx 0.8$ is probably due to problems in convincingly identifying quasars based on only MgII in the region of the dichroic split. We show ten selected spectra of the newly confirmed AGNs in Figure 4 and also show several spectra of common contaminating sources in Figure 5. The remaining spectra are discussed in Section 5, and

are either not quasars or quasars with too low S/N for clear detection. As we discuss in Section 6, a fair number of the fainter sources ($I \gtrsim 19$ mag) should be quasars.

One target, MQS J050155.46–700210.1, shows emission lines corresponding to redshifts of $z = 0.228$ and 0.341, as shown in Figure 6. This could be a chance coincidence or a gravitational lens. In the OGLE-III reference image (Figure 7), we find that the AGN candidate was a faint source ($V = 21.3$, $I = 20.5$) in the wings of a brighter extended source. The standard OGLE catalogs may not include all extended sources, so it is likely that the faint source was mistargeted and the brighter galaxy is the AGN candidate. If we assume the bright galaxy is acting as a gravitational lens, then we estimate that it has an Einstein radius of $R_E < 0.4$ arcsec, which is very small because of the small redshift difference. Higher resolution images and spatially resolved spectra are required to clarify the nature of this source.

5. CONTAMINANTS

For the sources that were not quasars, we used our spectra of the known sources to build template YSO, PN, blue/Be, and red star spectra, respectively, and fit them to the individual spectra. Apart from the automatic fits, we also visually inspected each spectrum. Table 5 reports the object type for each of the sources and Figure 5 shows examples of some of these sources. We briefly describe each type below.

Planetary nebulae. We classified sources as candidate PNe if they had roughly equally strong H α , H β , and/or [OIII] emission lines along with several additional lines such as HeI at 5876 \AA , 6680 \AA and 7065 \AA , HeII at 4686 \AA , [ArIII] at 7136 \AA , [NII] at 6548 \AA and 6584 \AA , [SII] 6716 \AA and 6731 \AA , and/or [ArIV] at 4711 \AA and 4740 \AA (see, e.g., Meatheringham & Dopita 1991). Of the 17 we classified as PNe based on our spectra, 7 were classified as such in SIMBAD and 5 were classified as YSOs.

Young stellar objects. We classified sources as candidate YSOs if they had significantly weaker [OIII] and H β lines relative to H α combined with relatively strong [SII] emission lines at 6716 \AA and 6731 \AA , [OI] at 6300 \AA , and/or [NII] at 6548 \AA and 6584 \AA (see, e.g., Kenyon et al. 1998). Of the 115 objects we classified as YSOs, 18 were classified as such by SIMBAD and 1 was classified as a PN, leaving 96 new candidate YSOs. There were also four additional sources we identify as YSO/PN where we were uncertain as to the correct classification. SIMBAD has two of these four classified as YSOs.

Be and blue stars. Blue stars had blue spectra with strong hydrogen Balmer series absorption. They were then further classed as Be stars if they had strong hydrogen H α (H β) emission lines. We identified 63 blue stars of which 39 appear to be Be stars. While there is little ambiguity about the Be stars, SIMBAD labels two of the blue stars without emission lines as PNe, one as a Mira-type star and one only as a Two Micron All Sky Survey (2MASS) infrared source (Cutri et al. 2003). We also found eight objects that could be either blue stars or YSOs. The median OGLE-III color of these blue stars is $(V - I) \simeq 0.1$ mag.

Red stars. These are stars with red spectra sometimes showing molecular absorption bands. We identified

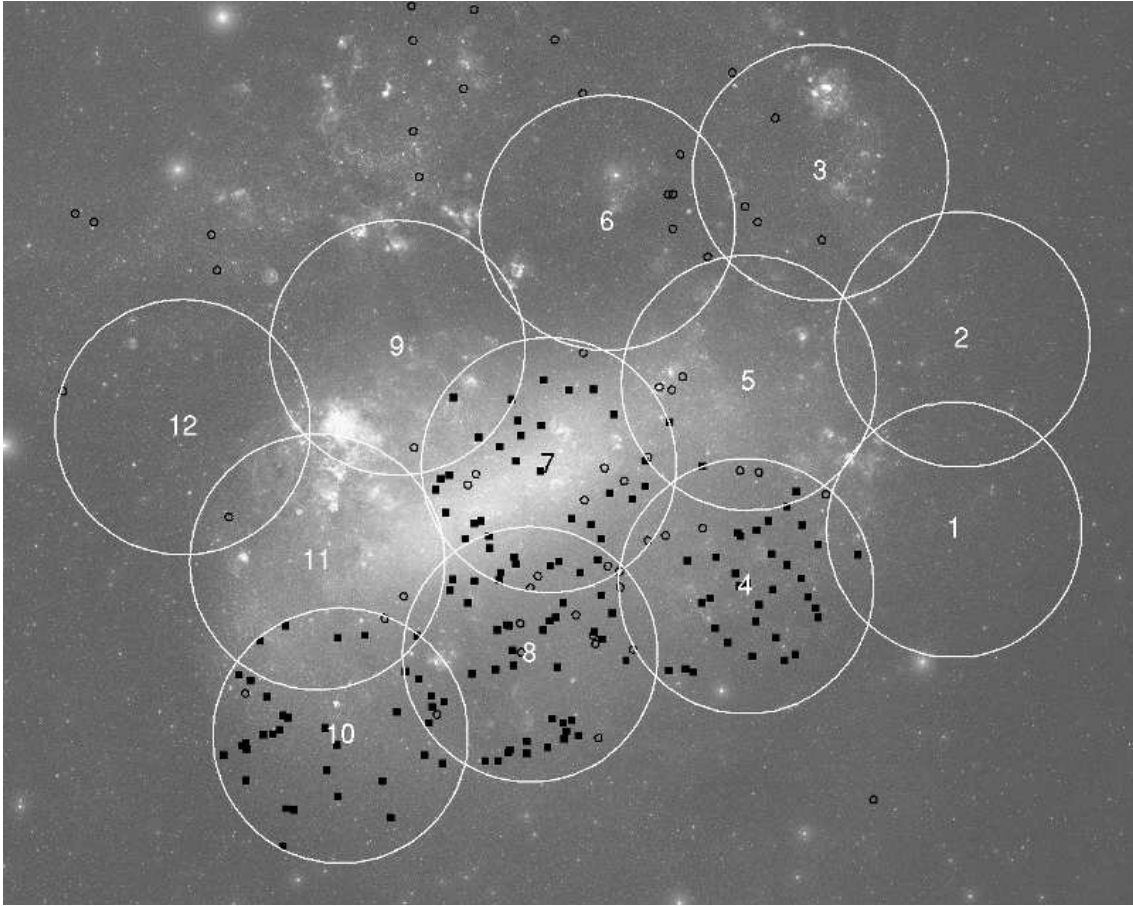


Figure 2. Twelve MQS LMC fields (large circles). The small open circles mark the previously known quasars behind the LMC, while the filled squares mark the 144 new quasars confirmed in this study. Due to bad weather we observed only four (4, 7, 8, and 10) of 12 planned fields. The image spans approximately $10 \text{ deg} \times 7 \text{ deg}$. North is up, east is to the left.

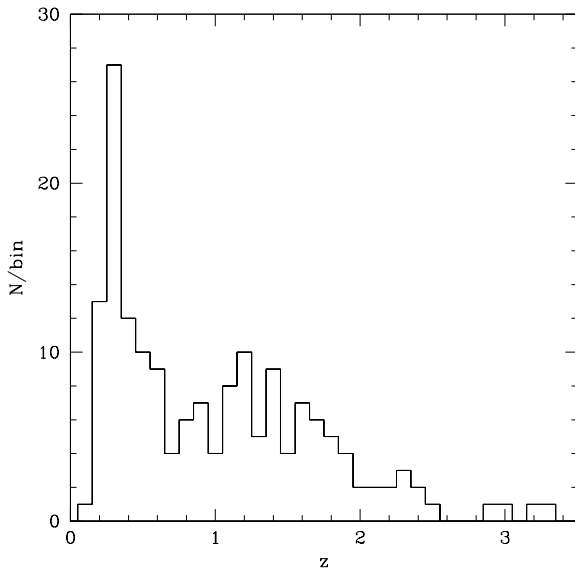


Figure 3. Redshift distribution of the confirmed quasars in $z = 0.1$ bins.

68 red sources, where SIMBAD classifies 4 as infrared sources (one YSO from Gruendl & Chu 2009 and three 2mass sources), 1 as a PN, 1 as a YSO, 1 as an asymptotic giant branch star, and 1 as a galaxy. The median

OGLE-III color of these sources is $(V - I) \simeq 1.1 \text{ mag}$.

6. DISCUSSION

The yield of our survey is determined by a combination of contamination and depth, where it is difficult to fully characterize the effects of depth because of the large variation in integration time created by the weather. For discussion, we simply combine the four fields (Table 2). We know from the surface density of candidates compared to quasars (Kochanek et al. 2011, Richards et al. 2006), shown in Figure 8, that the level of contamination is high, but much of this is by design because of the large number of available fibers.

In Figure 1 and Table 2, we present our yields from this observing run, divided by the selection method. The mid-IR-selected sources were divided into several classes (QSO-Aa, QSO-Ab, etc.; see Section 2.1). As expected the purest class, QSO-Aa, has the highest confirmation rate, at 24%. Next, the two classes QSO-Ab and QSO-Ba had confirmation rates of 20% and 19%, respectively. The YSO-Aa and YSO-Ab groups have lower rates of 13% and 6%, as expected from the original division into YSO and QSO classes. Variability selection had a yield of 31% and X-ray selection 30%.

Priority 7 objects, where the source was flagged based on only one of the mid-IR, variability or X-ray criteria, had confirmation rates of 13% (57 new AGNs), 7% (8), and 5% (1), respectively. Of the priority 8 objects se-

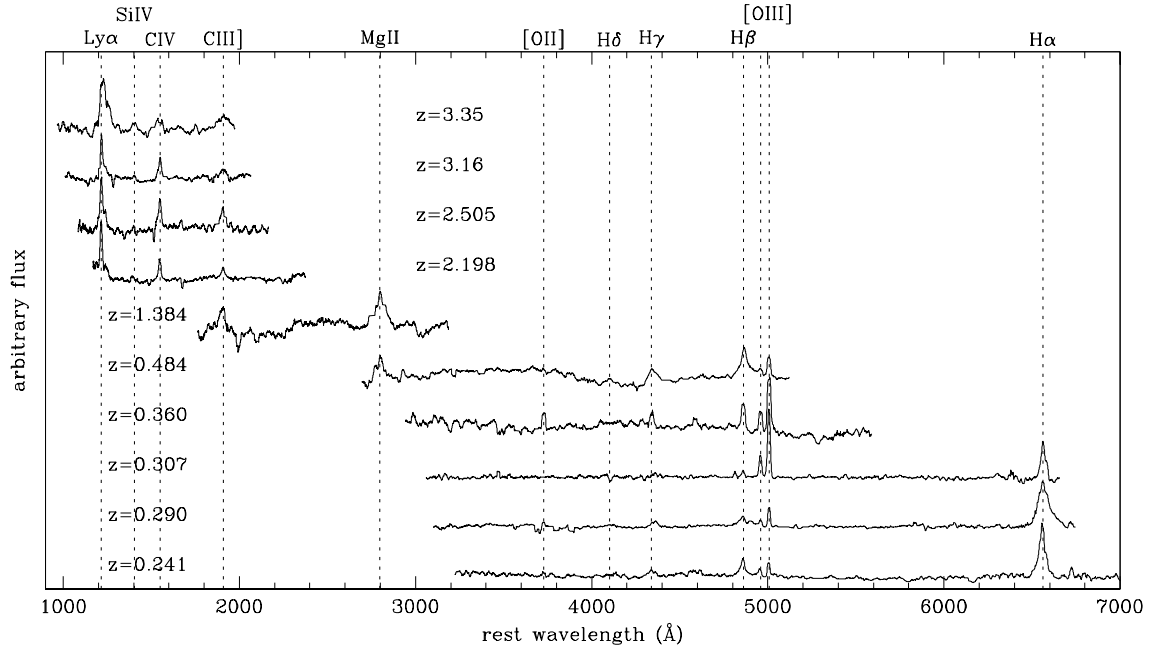


Figure 4. Ten of the 144 new LMC AGNs reported in this paper. The spectra have been flattened, smoothed, and scaled. The majority of the $z \approx 0$ LMC emission lines as well as the atmospheric absorption features have been masked in order to emphasize the quasar emission lines. Each spectrum is labeled by redshift and we also mark the common quasar lines (vertical dashed lines with labels).

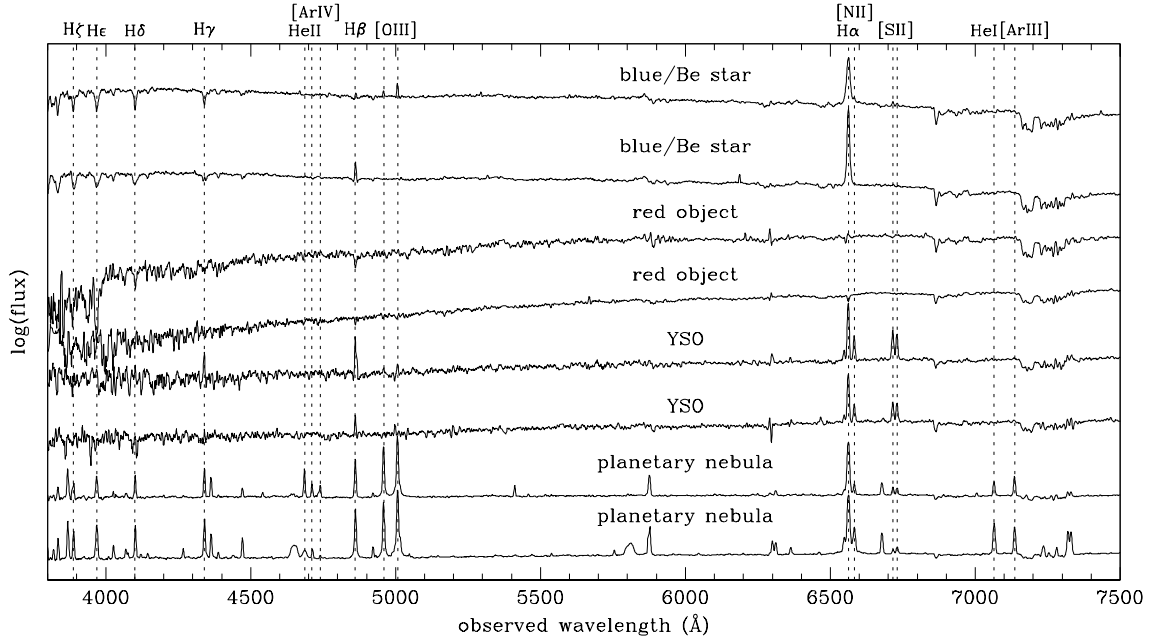


Figure 5. Common contaminants can be divided into four groups: PNe, YSOs, red objects, and blue/Be stars. We show two spectra for each class, and also mark basic lines (vertical dashed lines with labels).

lected by any two methods but not the third, the combination of X-ray plus variability yielded the highest confirmation rate, at 80% (4 new AGNs), most likely due to low number statistics. The mid-IR and variability criteria had a yield of 38% (73 AGNs) and X-ray plus mid-IR criteria had a yield of only 7%, again with low number statistics. Not surprisingly, combining all three selection methods was the most efficient with a yield of 65% (22 new AGNs).

Figure 8 shows the cumulative distribution of our targets and then their division into quasars, stars, and un-

classified objects. We also show the cumulative distribution of $z > 0.5$ quasars in AGES (Kochanek et al. 2011). These quasars are primarily mid-IR and X-ray selected, like much of the present sample, but with a much deeper optical spectroscopic limit. We have adjusted the AGES magnitudes for the $\Delta E(B - V) \simeq 0.14$ mag extinction difference between AGES and a typical LMC site line (Udalski et al. 1999), although this may underestimate the correction necessary for a true background population. The completeness of our present sample relative to AGES is roughly 50% (30%) at 18.6 mag (19.3 mag). Fig-

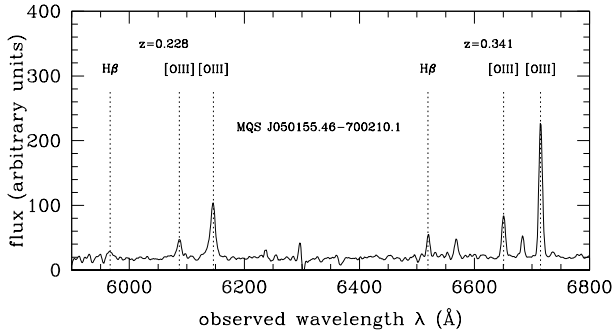


Figure 6. Spectrum for MQS J050155.46–700210.1. It displays two sets of the same emission lines at two redshifts, $z = 0.228$ and $z = 0.341$. We did not mask the LMC’s ISM lines [OI] (6300Å), H α (6563Å), and HeI (6678Å).

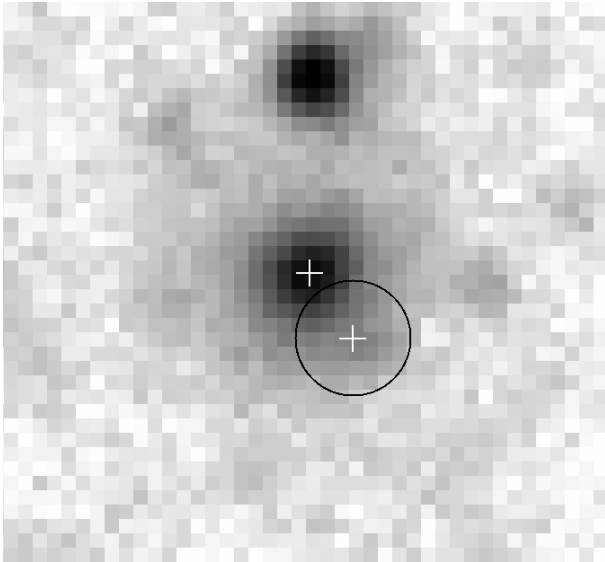


Figure 7. Finding chart for MQS J050155.46–700210.1. The circle has a diameter of 2 arcsec, corresponding to the AAOmega fiber size. The plus symbol inside the fiber marks the targeted source, while the plus symbol outside the fiber marks the galaxy, most likely hosting an AGN. The image is 10×10 arcsec. North is up, east is to the left.

ure 8 also shows the cumulative distribution of the SDSS quasars with $0.3 < z < 2.2$ from Richards et al. (2006). Given the change in bandpass (the $(i-I) \simeq 0.5$ mag color term varies significantly with redshift, see Figure 9) and the additional line width and luminosity selection criteria in Richards et al. (2006) it is harder to make a direct comparison, but after matching as best possible, we obtain similar completeness estimates. As expected from filling the fibers with targets, most targets are peculiar stars of various types, particularly at the brighter magnitudes. Unclassifiable spectra dominate at the fainter magnitudes, and with the weather-limited integration times, there was an effective magnitude limit of roughly 19.5–20 mag.

Figure 9 shows the colors of the confirmed quasars as a function of redshift. While we imposed no optical color selection criteria, the quasars generally follow the colors of SDSS quasars except at very low z , where the host dominates the colors. Adding an optical color constraint has no leverage on the selection of quasars, as the colors of quasars are indistinguishable from the colors of many

Table 2
MQS LMC Yields.

Selection	Observed Targets	Confirmed AGNs	Yield %
Mid-IR QSO-Aa	577	136 (137*)	24
Mid-IR QSO-Ab	10	2	20
Mid-IR QSO-Ba	62	12	19
Mid-IR QSO-Bb	1	0	0
Mid-IR YSO-Aa	32	4	13
Mid-IR YSO-Ab	16	1	6
Mid-IR YSO-Ba	1	0	0
Mid-IR YSO-Bb	3	0	0
Mid-IR (any)	702	155 (156*)	22
X-ray (any)	102	30	29
Var. (any)	350	107	31
X-ray + Mid-IR (any)	77	25	32
Mid-IR + Var. (any)	228	95	42
Var. + X-ray (any)	39	26	67
Priority 7			
Mid-IR (only)	431	57 (58*)	13
X-ray (only)	21	1	5
Var. (only)	117	8	7
Priority 8			
X-ray + Mid-IR (only)	43	3	7
Mid-IR + Var. (only)	194	73	38
Var. + X-ray (only)	5	4	80
Priority 9			
All three	34	22	65

Note. — *MQS J050155.46–700210.1 is consistent with having two redshifts (see, §4).

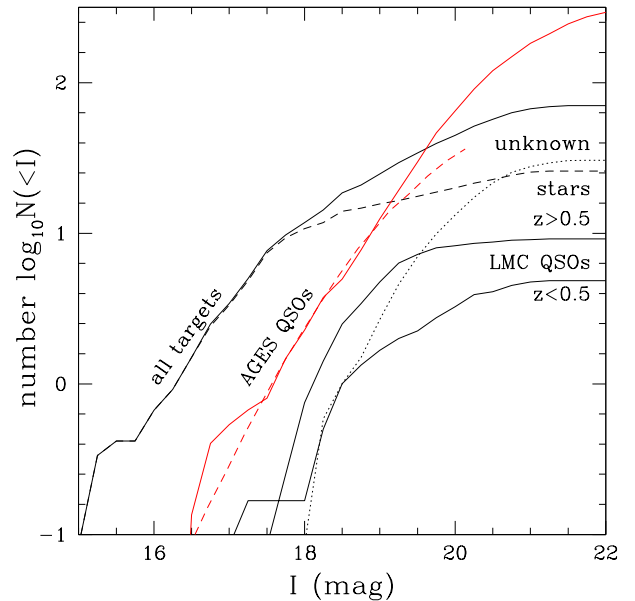


Figure 8. Cumulative distributions of MQS targets. The upper solid curve shows the distribution of all the targets, which is then decomposed into stars (dashed), unclassified spectra (dotted), and quasars (solid), divided into $z < 0.5$ and $z > 0.5$ sources). The red solid (dashed) curves show the distribution of $z > 0.5$ AGES (SDSS $0.3 < z < 2.2$) quasars for comparison. Our selection methods and bands are more comparable to AGES than to SDSS.

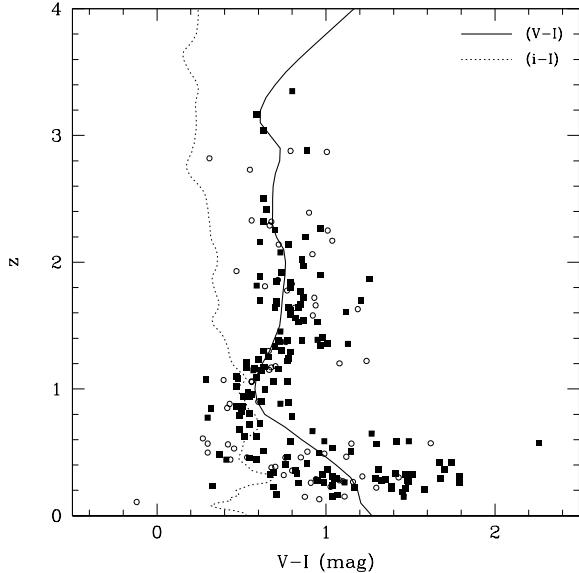


Figure 9. $V - I$ colors of the MQS LMC quasars (filled squares) and other confirmed LMC and SMC quasars (open circles) as a function of redshift. Overplotted is the color for a pure AGN spectrum from Vanden Berk et al. (2001) convolved with the V and I filters (solid line). The same spectrum was also convolved with the i and I filters in order to convert OGLE magnitudes into SDSS i -band magnitudes—the $(i - I)$ color is shown as dotted line.

LMC stars.

In Figures 10–12, we examine the selection spaces used to select the candidates. First, we inspect the $\tau - \hat{\sigma}$ variability plane from Kozłowski et al. (2010a) and MacLeod et al. (2010). Kozłowski et al. (2010a) proposed a narrow and long trapezoidal region to select high purity sample of AGN candidates. Indeed, if we had restricted our variability selection to this region, we would have a yield of 70% at the price of a significant reduction in completeness. In fact, the distribution of the variability parameters of all quasars follows the distribution found by MacLeod et al. (2010) for SDSS quasars, extending outside the Kozłowski et al. (2010a) selection boundaries, particularly for long τ where there is also increased contamination from irregularly varying stars. The left panel of Figure 10 shows the distribution of objects classified as non-quasars (PNe, YSOs, etc.) or where we failed to classify the spectrum in this variability plane. We note that the vast majority of classified non-quasars lie outside the Kozłowski et al. (2010a) region.

In Figure 11, we make the same comparison between the MQS quasars and the other candidates in the $A - \gamma$ variability plane of Schmidt et al. (2010). We used a cut in this plane to remove more variable sources (shown as contours) other than quasars that we included as we greatly relaxed the DRW selection criteria of Kozłowski et al. (2010a) in these dense stellar fields. A fair number of common variable stars are periodic with the index of the power-law SF of $\gamma < 0.1$. On the other hand, objects with very high amplitude variations are unlikely to be quasars as quasar variability amplitudes on long time-scales are expected to be $A \approx 0.3$ mag (e.g., MacLeod et al. 2010). Our simple cut (solid lines) allows higher contamination than that of Schmidt et al. (2010,

dotted lines), but also returns the higher number of confirmed quasars.

We also examined the distribution of the confirmed MQS quasars and quasar candidates relative to the mid-IR selection criteria of Kozłowski & Kochanek (2009, Figure 12). The quasars lie in the proposed selection regions confirming the basic principles outlined in Kozłowski & Kochanek (2009). The remaining quasar candidates (shown in the left panels) are either quasars with low S/N or contaminating sources. In the mid-IR color-color plot (top panels in Figure 12), the confirmed quasars (shown in the right panel) and the faint candidates (gray squares in the left panel) occupy nearly identical regions, while the blue and red stars tend to clump in the lower-left region of the “AGN wedge” area. Also, YSOs tend to have a somewhat larger color spread than the more centrally clumped AGNs. In the mid-IR CMD (middle panels of Figure 12), the confirmed quasars seem to be on average brighter than the remaining faint sources. The red stars tend to have bluer mid-IR $[3.6] - [8.0]$ colors than the other sources. In the bottom panels of Figure 12, we show the optical-to-mid-IR colors of our observed targets. As expected the vast majority of our quasars occupy the “a” (QSO-like optical-to-mid-IR colors) region, but then so do the most of other sources. The red stars again have bluer optical-to-mid-IR colors than the other sources.

As expected from earlier surveys of mid-IR-selected quasars (Stern et al. 2005; Assef et al. 2010), we find that 88% of the mid-IR-selected quasars show optical broad lines and are not Type II quasars. Similarly, of the 155 confirmed, mid-IR-selected quasars, 95 (61%) are clearly variable sources.

7. SUMMARY

We observed 845 AGN candidates in four ~ 3 deg² LMC fields with AAOmega to confirm 169 quasars, including 144 new ones. Given the 55 previously known quasars behind the LMC, including 25 in our present fields, we have quadrupled (to 200) the number of known quasars behind the LMC. By observing the eight remaining fields, we should find another ~ 300 new quasars, although the yield would increase if all data were obtained with the full integration time.

We observed the quasar candidates based on the priorities set by the number of the selection methods that picked them. If they were selected by only one method, either mid-IR colors, X-ray emission, or photometric variability, the average confirmation yield is low, at $\sim 9\%$. If the candidate was selected based on two methods but not the third, the average confirmation rate is at 40%. The highest yields come with the simultaneous selection by all three methods, with the yield at 65%. Note, however, that we deliberately chose to fill all the AAOmega fibers with candidates in order to achieve higher completeness, guaranteeing high contamination rates because the surface density of quasars is well below the surface density of fibers.

Our biggest problem given the availability of fibers is not contamination. We could assign rough classifications to many contaminating sources, including 115 YSOs (96 new), 17 PNe (5 new), 39 new Be and 24 blue stars, 68 red stars, and also 12 objects that are either YSO/PN or blue star/YSO. The big problem is that we could not

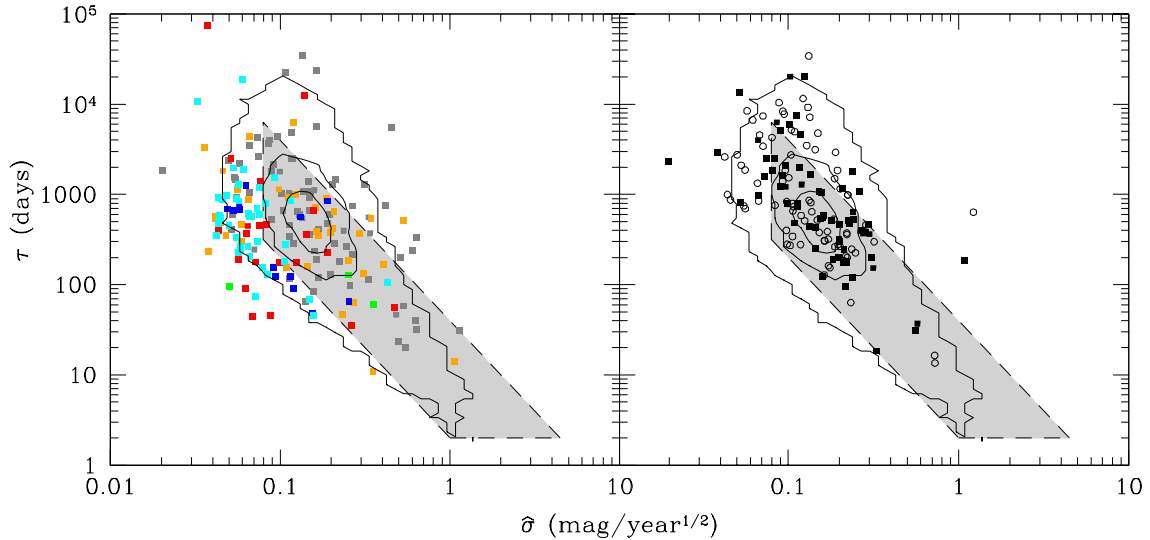


Figure 10. τ - δ (timescale–scaled amplitude) variability plane. In the left panel, we show the observed variable AGN candidates that are not quasars. They are YSOs (orange), blue stars (blue), red stars (red), PNe (green), Be stars (cyan), and objects with featureless spectra (dark gray). In the right panel, we show the confirmed MQS LMC quasars (filled squares) and other known LMC and SMC quasars (open circles) as compared to the selection criteria in Kozłowski et al. (2010a) (gray area) and density contours (1, 10, and 20 per 0.1 dex bins in both axes) for ~ 9000 variable SDSS AGNs from MacLeod et al. (2010). The Kozłowski et al. (2010a) cut was designed to return high purity samples given the variability properties of contaminating stars. With plenty of fibers, however, we significantly extended this selection region (see Section 2.3).

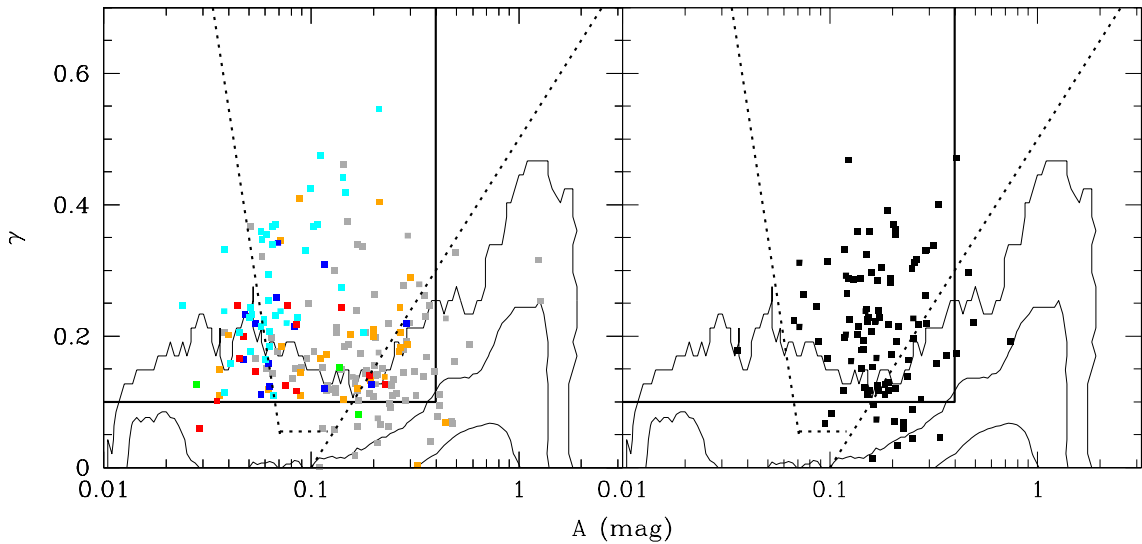


Figure 11. A - γ (amplitude–structure function slope) variability plane from Schmidt et al. (2010). In the left panel, we show the observed variable AGN candidates that are not quasars. Color coding is as in Figure 10. In the right panel, we show the confirmed MQS LMC quasars (filled squares). Our selection region is above the horizontal ($\gamma > 0.1$) and left of the vertical ($A < 0.4$ mag) solid lines. Some of our new confirmed quasars and quasar candidates are outside this cut—these are objects selected by methods other than variability. The dashed lines are the selection cuts from Schmidt et al. (2010). The contours are for $\sim 30,000$ variable objects from a 1 deg^2 area with the typical stellar density of the LMC. The objects are counted in $\Delta A = 0.02$ dex and $\Delta \gamma = 0.02$ bins. The outer, middle, and inner contours are for 1, 10, and 100 objects per bin, respectively.

classify 402 spectra due to low S/N, what is also a major problem for making black hole mass estimates from the line widths of the quasar emission lines.

Nonetheless, tripling the number of quasars in the LMC and SMC using only 5 hr on sky is a strong vindication of the general approach and the advantages created by the large numbers of AAOmega fibers. With no improvements in yields due to actually obtaining our target integration times, we estimate that completing the OGLE-III LMC and SMC fields would yield ~ 700 quasars and completing the OGLE-IV fields would yield ~ 3600 quasars. These remain the best fields for extend-

ing studies of quasar variability independent of their additional uses for understanding the Galaxy through the proper motions of the LMC or probing the local ISM.

We thank Sarah Brough, our support astronomer, for help during the observing run. We thank Michał Jaroszyński for the helpful discussion on MQS J050155.46–700210.1. We also thank the anonymous referee, whose comments helped us to improve the manuscript. This research was made based on observations with the Anglo-Australian Telescope, for which

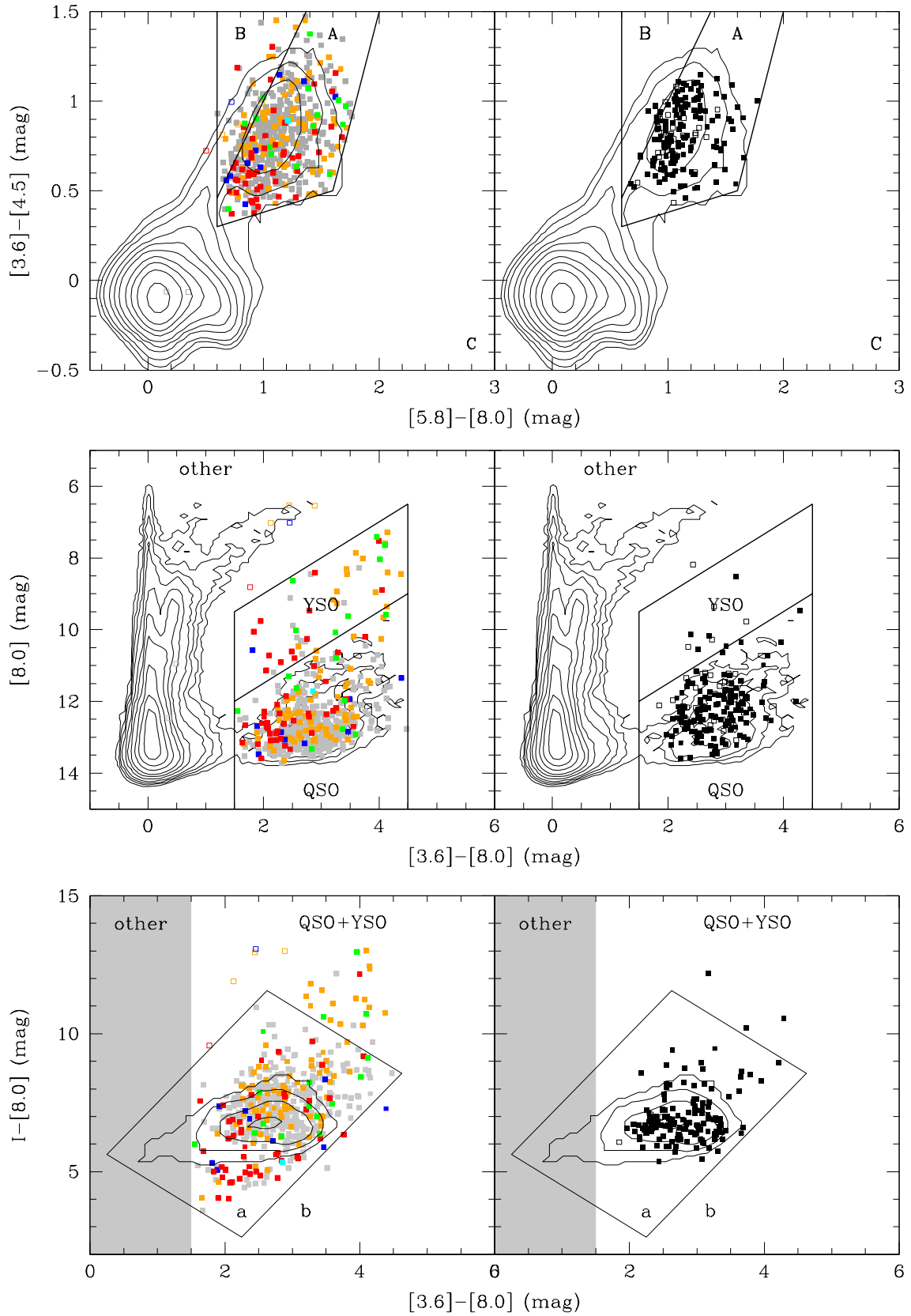


Figure 12. AGN selection criteria from Kozłowski & Kochanek (2009). These cuts are summarized in Section 2.1. In the left panels, the filled symbols mark the mid-IR-selected confirmed YSOs (orange), blue stars (blue), red stars (red), PNe (green), Be star (cyan) and objects with featureless spectra (gray), while the open symbols are for the candidates selected by the variability and/or X-ray selection method and then matched to the *Spitzer* and OGLE-III data. In the right panels, the filled symbols mark the confirmed quasars from this work (both new and known) and the open symbols are for the other known LMC quasars, that are outside of the four observed fields.

the observing time was granted by the Optical Infrared Coordination Network for Astronomy (OPTICON). This research has made use of the SIMBAD database, operated at CDS, Strasbourg, France. This research has also made use of the NASA/IPAC Extragalactic Database (NED) which is operated by the Jet Propulsion Laboratory (JPL), California Institute of Technology (Caltech), under contract with the National Aeronautics and Space Administration (NASA).

Support for this work was provided by the Polish Ministry of Science and Higher Education (MNiSW) through the program “Iuventus Plus”, award number IP2010 020470 to S.K., A.M.J., and A.U. This work has been supported by NSF grants AST-0708082 and AST-1009756 to C.S.K. The OGLE is supported by the European Research Council under the European Community’s Seventh Framework Programme (FP7/2007-2013), ERC grant agreement no. 246678 to A.U.

REFERENCES

- Alcock, C., et al. 2000, *ApJ*, 542, 281
 Ashby, M. L. N., et al. 2009, *ApJ*, 701, 428
 Assef, R. J., et al. 2010, *ApJ*, 713, 970
 Assef, R. J., et al. 2011, *ApJ*, 728, 56
 Butler, N. R., & Bloom, J. S. 2011, *AJ*, 141, 93
 Clocchiatti, A., et al. 2003, *IAU Circ.*, 8258, 1
 Crampton, D., Gussie, G., Cowley, A. P., & Schmidtke, P. C. 1997, *AJ*, 114, 2353
 Cutri, R. M., et al. 2003, *VizieR Online Data Catalog*, 2246, 0
 Dobrzycki, A., Groot, P. J., Macri, L. M., & Stanek, K. Z. 2002, *ApJ*, 569, L15
 Dobrzycki, A., Macri, L. M., Stanek, K. Z., & Groot, P. J. 2003a, *AJ*, 125, 1330
 Dobrzycki, A., Stanek, K. Z., Macri, L. M., & Groot, P. J. 2003b, *AJ*, 126, 734
 Dobrzycki, A., Eyer, L., Stanek, K. Z., & Macri, L. M. 2005, *A&A*, 442, 495
 Eisenhardt, P. R., et al. 2004, *ApJS*, 154, 48
 Geha, M., et al. 2003, *AJ*, 125, 1
 Gorjian, V., et al. 2008, *ApJ*, 679, 1040
 Gruendl, R. A., & Chu, Y.-H. 2009, *ApJS*, 184, 172
 Haberl, F., & Pietsch, W. 1999, *A&AS*, 139, 277
 Ivezić, Z., et al. 2008, arXiv:0805.2366
 Kaiser, N., et al. 2002, *Proc. SPIE*, 4836, 154
 Kallivayalil, N., et al., 2006, *ApJ*, 638, 772
 Kelly, B. C., Bechtold, J., & Siemiginowska, A. 2009, *ApJ*, 698, 895
 Kenyon, S. J., Brown, D. I., Tout, C. A., & Berlind, P. 1998, *AJ*, 115, 2491
 Kochanek, C. S., Eisenstein, D. J., Cool, R. J., et al. 2011, arXiv:1110.4371
 Kozłowski, S., & Kochanek, C. S. 2009, *ApJ*, 701, 508
 Kozłowski, S., et al. 2010a, *ApJ*, 708, 927
 Kozłowski, S., et al. 2010b, *ApJ*, 716, 530
 Kozłowski, S., Kochanek, C. S., & Udalski, A. 2011, *ApJS*, 194, 22
 Lacy, M., et al. 2004, *ApJS*, 154, 166
 MacLeod, C. L., et al. 2010, *ApJ*, 721, 1014
 MacLeod, C. L., et al. 2011, *ApJ*, 728, 26
 Meatheringham, S. J., & Dopita, M. A. 1991, *ApJS*, 75, 407
 Meixner, M., et al. 2006, *AJ*, 132, 2268
 Noda, S., et al. 2002, *MNRAS*, 330, 137
 Piatek, S., Pryor, C., & Olszewski, E. W., 2008, *AJ*, 135, 1024
 Richards, G. T., et al. 2006, *AJ*, 131, 2766
 Sasaki, M., Haberl, F., & Pietsch, W. 2000, *A&AS*, 143, 391
 Schmidt, K. B., Marshall, P. J., Rix, H.-W., Jester, S., Hennawi, J. F., & Dobler, G. 2010, *ApJ*, 714, 1194
 Schmidtke, P. C., Cowley, A. P., Frattare, L. M., McGrath, T. K., Hutchings, J. B., & Crampton, D. 1994, *PASP*, 106, 843
 Sharp, R., et al. 2006, *Proc. SPIE*, 6269,
 Stern, D., et al. 2005, *ApJ*, 631, 163
 Taylor, K., Bailey, J., Wilkins, T., Shortridge, K., & Glazebrook, K. 1996, *Astronomical Data Analysis Software and Systems V*, 101, 195
 Udalski, A., Szymanski, M., Kubiak, M., et al. 1999, *Acta Astron.*, 49, 201
 Udalski, A., Szymański, M. K., Soszyński, I., & Poleski, R. 2008a, *Acta Astron.*, 58, 69
 Udalski, A., et al. 2008b, *Acta Astron.*, 58, 89
 Vanden Berk, D. E., et al. 2001, *AJ*, 122, 549
 Whitney, B. A., et al., 2008, *AJ*, 136, 18

TABLE 3
PARAMETERS OF 144 NEW AGNs BEHIND THE LMC.

Name	R.A.	Decl.	V (mag)	I (mag)	z	OGLE-III ID	KK09 Class	Emission Lines	Mid-IR	X-Ray	Var.	Notes
MQS J045027.59-700755.2	4:50:27.59	-70:07:55.2	20.10	19.60	0.820	lmc137.5.15321	QSO-Aa	MgII, [OII]	Y	...	Y	...
MQS J045340.07-704014.4	4:53:40.07	-70:40:14.4	99.99	20.65	0.537	lmc137.1.14392	QSO-Aa	H $\delta\gamma\beta$, [OIII]	Y
MQS J045358.18-703542.0	4:53:58.18	-70:35:42.0	19.70	18.96	1.920	lmc137.1.11175	QSO-Aa	CIV, CIII	Y	...	Y	...
MQS J045417.37-700510.0	4:54:17.37	-70:05:10.0	19.01	18.29	1.384	lmc136.1.15296	QSO-Aa	CIII], MgII	Y	...	Y	...
MQS J045448.25-703040.1	4:54:48.25	-70:30:40.1	19.58	18.79	1.291	lmc137.2.14446	QSO-Aa	CIII], MgII	Y	...	Y	...
MQS J045536.48-705852.2	4:55:36.48	-70:58:52.2	19.89	18.92	1.901	lmc130.6.2119	...	CIV, CIII]	Y	...
MQS J045538.32-702202.5	4:55:38.32	-70:22:02.5	20.62	19.83	1.841	lmc129.6.4452	QSO-Aa	CIV, MgII	Y	...	Y	...
MQS J045554.81-695612.5	4:55:54.81	-69:56:12.5	19.23	18.37	1.386	lmc128.7.275	QSO-Aa	CIII], MgII	Y	...	Y	...
MQS J045636.71-710226.2	4:56:36.71	-71:02:26.2	18.77	17.82	1.526	lmc130.7.12991	QSO-Aa	CIII], MgII	Y	...	Y	...
MQS J045645.86-694017.8	4:56:45.86	-69:40:17.8	20.85	19.37	0.275	lmc128.5.7243	QSO-Aa	[OII], H $\delta\beta$, [OIII], H α	Y	...	Y	...
MQS J045707.11-701609.7	4:57:07.11	-70:16:09.7	99.99	20.71	0.485	lmc129.5.28199	QSO-Aa	[OII], H β , [OIII]	Y
MQS J045731.81-694756.4	4:57:31.81	-69:47:56.4	19.80	19.28	0.627	lmc128.6.12391	QSO-Aa	MgII, [OII], [OIII]	Y	...	Y	...
MQS J045736.84-705126.9	4:57:36.84	-70:51:26.9	19.04	18.75	1.079	lmc130.5.17707	QSO-Aa	MgII	Y	...	Y	...
MQS J045819.29-702826.4	4:58:19.29	-70:28:26.4	21.76	20.27	0.588	lmc129.7.27692	QSO-Aa	[OII], H β , [OIII]	Y
MQS J045836.95-701120.2	4:58:36.95	-70:11:20.2	18.69	18.14	0.938	lmc129.4.939	QSO-Aa	MgII, [OII]	Y	...	Y	YSO
MQS J045907.78-695516.2	4:59:07.78	-69:55:16.2	19.48	18.77	1.674	lmc128.2.657	QSO-Ba	CIV, CIII, MgII	Y	...	Y	...
MQS J045931.28-703622.1	4:59:31.28	-70:36:22.1	20.87	19.91	0.493	lmc129.1.4245	QSO-Aa	[OII], [OIII]	Y	...	Y	...
MQS J045943.60-704430.9	4:59:43.60	-70:44:30.9	19.76	19.06	2.254	lmc130.4.21594	QSO-Aa	Ly α , CIV, CIII]	Y	...	Y	...
MQS J045951.22-710118.4	4:59:51.22	-71:01:18.4	18.71	18.34	0.484	lmc130.2.13285	QSO-Ba	MgII, [OII], H $\delta\gamma\beta$, [OIII]	Y	...	Y	...
MQS J050010.83-700028.5	5:00:10.83	-70:00:28.5	20.87	19.17	0.365	lmc128.1.30448	QSO-Aa	[OII], [OIII]	Y
MQS J050044.85-702606.3	5:00:44.85	-70:26:06.3	21.38	20.17	1.697	lmc129.2.22770	QSO-Aa	CIV, CIII], MgII	Y	...	Y	...
MQS J050130.73-702751.2	5:01:30.73	-70:27:51.2	21.49	20.10	0.238	lmc129.2.25178	QSO-Aa	[OII], H β , [OIII], H α	Y
MQS J050139.74-700344.2	5:01:39.74	-70:03:44.2	19.15	18.31	0.258	lmc128.1.36694	QSO-Aa	H $\gamma\beta$ [OIII], H α	Y	...	Y	...
MQS J050155.26-700209.6(a)	5:01:55.46	-70:02:10.1	19.54	17.72	0.228	lmc128.1.44266	QSO-Aa	[OII], H β , [OIII], H α	Y
MQS J050155.26-700209.6(b)	5:01:55.46	-70:02:10.1	19.54	17.72	0.341	lmc128.1.44266	QSO-Aa	[OII], H β , [OIII], H α	Y
MQS J050155.31-702149.7	5:01:55.31	-70:21:49.7	21.41	19.94	0.324	lmc129.3.29542	QSO-Aa	H $\gamma\beta$ [OIII], H α	Y
MQS J050219.37-705533.1	5:02:19.37	-70:55:33.1	20.40	19.53	1.971	lmc122.6.2550	QSO-Aa	CIV, CIII]	Y	...	Y	...
MQS J050338.85-704907.9	5:03:38.85	-70:49:07.9	20.57	19.80	0.461	lmc122.5.24297	QSO-Aa	H β , [OIII]	Y
MQS J050355.36-701434.5	5:03:55.36	-70:14:34.5	21.11	20.28	0.333	lmc121.5.18749	QSO-Aa	[OII], [OIII], H α	Y
MQS J050417.46-703432.1	5:04:17.46	-70:34:32.1	20.51	19.88	1.175	lmc121.7.13362	QSO-Ba	CIII], MgII	Y
MQS J050503.98-703650.5	5:05:03.98	-70:36:50.5	19.79	19.08	1.850	lmc121.8.38622	QSO-Aa	CIV, CIII], MgII	Y	...
MQS J050532.72-693046.1	5:05:32.72	-69:30:46.1	99.99	20.92	0.158	lmc119.8.41486	QSO-Ab	[OII], H β , [OIII], H α	Y	YSO
MQS J050536.08-711053.5	5:05:36.08	-71:10:53.5	19.14	18.53	1.888	lmc122.1.1849	QSO-Aa	CIV, CIII], MgII	Y	...	Y	...
MQS J050625.44-710907.8	5:06:25.44	-71:09:07.8	20.37	19.64	1.454	lmc122.2.4735	QSO-Ba	CIII], MgII	Y
MQS J050637.14-701642.4	5:06:37.14	-70:16:42.4	18.95	18.16	0.586	lmc121.4.8554	YSO-Aa	MgII, [OII], H β , [OIII]	Y	...	Y	...
MQS J050804.91-711027.0	5:08:04.91	-71:10:27.0	19.31	18.70	2.160	lmc122.1.16417	QSO-Aa	Ly α , SiIV, CIV, CIII]	Y
MQS J050842.68-690959.4	5:08:42.68	-69:09:59.4	19.91	19.31	1.234	lmc119.3.99943	...	CIII], MgII	Y	...
MQS J051045.85-694126.5	5:10:45.85	-69:41:26.5	19.06	18.37	1.061	lmc112.6.70255	QSO-Aa	MgII	Y	...	Y	...
MQS J051049.16-692851.9	5:10:49.16	-69:28:51.9	21.73	19.94	0.307	lmc111.8.15536	QSO-Aa	[OII], H β , [OIII], Ha	Y	YSO
MQS J051159.38-694726.1	5:11:59.38	-69:47:26.1	99.99	20.64	0.289	lmc112.6.40559	QSO-Aa	[OII], [OIII], H α	Y
MQS J051221.49-710555.6	5:12:21.49	-71:05:55.6	99.99	20.70	0.286	lmc114.2.5479	YSO-Ab	[OII], [OIII], H α	Y	YSO
MQS J051345.50-690636.9	5:13:45.50	-69:06:36.9	20.65	19.59	0.290	lmc111.3.64618	QSO-Aa	[OII], [OIII], H α	Y
MQS J051347.16-704253.2	5:13:47.16	-70:42:53.2	19.64	18.63	0.368	lmc113.1.8170	QSO-Aa	[OII], H β , [OIII]	Y	...	Y	...
MQS J051404.81-694446.6	5:14:04.81	-69:44:46.6	20.28	19.31	0.723	lmc112.3.72688	QSO-Ba	MgII, [OII], [OIII]	Y	...	Y	...
MQS J051447.67-705548.3	5:14:47.67	-70:55:48.3	19.99	19.15	1.526	lmc114.3.19666	QSO-Aa	CIII], MgII	Y	...	Y	...
MQS J051453.74-703413.8	5:14:53.74	-70:34:13.8	21.48	19.81	0.421	lmc113.2.27595	QSO-Aa	[OII], H β , [OIII]	Y	YSO
MQS J051453.79-700705.3	5:14:53.79	-70:07:05.3	20.34	18.87	0.323	lmc112.1.19543	QSO-Aa	H β , [OIII], H α	Y	Y	Y	...
MQS J051509.61-701711.7	5:15:09.61	-70:17:11.7	20.92	20.36	0.955	lmc113.3.70911	QSO-Aa	MgII	Y
MQS J051533.21-705155.1	5:15:33.21	-70:51:55.1	22.05	20.75	0.565	lmc114.4.34927	QSO-Aa	[OII], [OIII]	Y
MQS J051534.35-685422.2	5:15:34.35	-68:54:22.2	21.77	20.03	0.417	lmc110.1.36621	QSO-Aa	[OII], [OIII]	Y	YSO
MQS J051547.78-700002.3	5:15:47.78	-70:00:02.3	19.89	19.04	1.769	lmc112.1.66457	QSO-Aa	CIV, CIII]	Y	Y
MQS J051654.08-702315.3	5:16:54.08	-70:23:15.3	18.20	17.40	3.35	lmc104.6.8162	QSO-Aa	Ly α , SiIV, CIV	Y	...	Y	YSO
MQS J051709.98-714212.4	5:17:09.98	-71:42:12.4	19.20	18.50	1.643	lmc106.7.14709	QSO-Aa	CIV, CIII], MgII	Y	...	Y	...
MQS J051739.83-695705.3	5:17:39.83	-69:57:05.3	22.34	20.08	0.575	lmc103.7.25537	QSO-Aa	[OII], H β , [OIII]	Y	YSO

TABLE 3 — *Continued*

Name	R.A.	Decl.	<i>V</i> (mag)	<i>I</i> (mag)	<i>z</i>	OGLE-III ID	KK09 Class	Emission Lines	Mid-IR	X-Ray	Var.	Notes
MQS J051746.88–685458.1	5:17:46.88	−68:54:58.1	20.13	19.14	0.588	lmc101.8.29032	QSO-Aa	MgII, [OII], H β , [OIII]	Y	Y	Y	...
MQS J051751.40–713507.2	5:17:51.40	−71:35:07.2	19.20	18.73	1.023	lmc106.6.15269	QSO-Aa	MgII	Y	...	Y	...
MQS J051822.78–714008.2	5:18:22.78	−71:40:08.2	21.38	20.07	0.363	lmc106.7.22303	QSO-Aa	[OII], H β , [OIII]	Y
MQS J051834.75–703751.3	5:18:34.75	−70:37:51.3	20.42	19.64	0.895	lmc104.8.49923	QSO-Aa	MgII	Y
MQS J051838.54–714402.2	5:18:38.54	−71:44:02.2	18.89	18.11	2.139	lmc106.7.14447	QSO-Aa	SiIV, CIV, CIII]	Y	...	Y	...
MQS J051842.63–713614.0	5:18:42.63	−71:36:14.0	18.82	18.34	1.080	lmc106.6.16038	QSO-Aa	MgII	Y	Y	Y	...
MQS J051856.04–701743.6	5:18:56.04	−70:17:43.6	19.22	18.71	0.863	lmc104.6.59124	QSO-Aa	MgII, [OII]	Y	...	Y	...
MQS J051912.33–710914.6	5:19:12.33	−71:09:14.6	21.15	20.11	0.306	lmc105.2.1048	QSO-Aa	[OII], H β , [OIII], H α	Y
MQS J051916.98–704458.8	5:19:16.98	−70:44:58.8	19.32	18.48	1.645	lmc105.4.25865	QSO-Aa	CIV, CIII], MgII	Y	...	Y	...
MQS J051944.39–701957.3	5:19:44.39	−70:19:57.3	20.05	19.50	0.809	lmc104.3.40092	QSO-Aa	MgII, [OII]	Y	...	Y	...
MQS J051952.01–713358.4	5:19:52.01	−71:33:58.4	22.10	21.06	0.537	lmc106.3.13325	QSO-Aa	[OII], H δ - γ β , [OIII]	Y
MQS J051953.65–704622.7	5:19:53.65	−70:46:22.7	20.75	19.49	1.865	lmc105.4.32704	QSO-Aa	SiIV, CIV, CIII], MgII	Y	...	Y	...
MQS J052004.67–684945.8	5:20:04.67	−68:49:45.8	99.99	20.97	0.480	lmc101.1.61308	QSO-Ba	[OII], H β , [OIII]	Y
MQS J052018.82–691137.7	5:20:18.82	−69:11:37.7	19.35	18.72	0.509	lmc100.3.18491	QSO-Aa	MgII, [OII], H δ β , [OIII]	Y	Y	Y	...
MQS J052021.61–714756.5	5:20:21.61	−71:47:56.5	21.61	20.12	0.269	lmc106.1.8704	QSO-Aa	H β , [OII], H α	Y
MQS J052030.99–693355.6	5:20:30.99	−69:33:55.6	20.76	19.41	0.289	lmc103.4.91031	QSO-Aa	H β , [OIII], H α	Y	YSO
MQS J052037.03–705100.1	5:20:37.03	−70:51:00.1	21.20	19.69	0.327	lmc105.4.7777	QSO-Aa	[OII], H β , [OIII], H α	Y
MQS J052211.42–691633.2	5:22:11.42	−69:16:33.2	21.22	20.07	0.506	lmc161.7.63819	QSO-Aa	[OII], [OIII]	Y
MQS J052227.15–690905.0	5:22:27.15	−69:09:05.0	19.82	18.78	0.241	lmc161.6.49171	QSO-Aa	[OII], H β , [OIII], H α	Y	Y	Y	...
MQS J052229.81–715037.3	5:22:29.81	−71:50:37.3	19.69	19.06	3.04	lmc106.1.18127	QSO-Aa	Ly α , SiIV, CIV, CIII]	Y	...	Y	...
MQS J052230.13–714500.3	5:22:30.13	−71:45:00.3	19.51	18.98	1.215	lmc106.2.18102	...	CIII], MgII	Y	HMXB/YSO
MQS J052245.80–692835.7	5:22:45.80	−69:28:35.7	19.49	18.73	0.406	lmc161.8.70581	QSO-Aa	[OIII]	Y	Y
MQS J052259.14–685849.0	5:22:59.14	−68:58:49.0	20.11	18.98	1.355	lmc161.5.48055	QSO-Aa	CIII], MgII	Y	...	Y	...
MQS J052300.14–701831.7	5:23:00.14	−70:18:31.7	19.69	19.22	1.100	lmc163.6.52005	QSO-Aa	CIII], MgII	Y	...	Y	...
MQS J052312.95–701529.8	5:23:12.95	−70:15:29.8	20.24	18.95	0.290	lmc163.5.2807	QSO-Ba	[OII], H β , [OIII], H α	Y	Y	Y	...
MQS J052335.33–710758.1	5:23:35.33	−71:07:58.1	19.97	19.24	0.883	lmc164.7.6854	QSO-Aa	MgII	Y	...	Y	...
MQS J052336.58–710033.9	5:23:36.58	−71:00:33.9	20.05	18.93	1.610	lmc164.6.6840	QSO-Aa	CIV, CIII], MgII	Y	...	Y	...
MQS J052354.44–704821.9	5:23:54.44	−70:48:21.9	20.16	19.58	1.160	lmc164.5.8392	QSO-Aa	CIII], MgII	Y	Y	Y	...
MQS J052408.88–704812.8	5:24:08.88	−70:48:12.8	19.66	18.79	1.541	lmc164.5.7759	QSO-Aa	CIV, CIII], MgII	Y	Y	Y	...
MQS J052411.14–692126.7	5:24:11.14	−69:21:26.7	18.45	17.68	1.061	lmc161.7.32441	YSO-Aa	CIII], MgII	Y	...	Y	YSO
MQS J052413.46–714843.6	5:24:13.46	−71:48:43.6	20.05	19.52	1.167	lmc165.8.24292	QSO-Aa	CIII], MgII	Y
MQS J052426.23–715003.6	5:24:26.23	−71:50:03.6	19.73	18.93	0.781	lmc165.8.23784	QSO-Aa	MgII, [OII], H γ β	Y	...	Y	...
MQS J052431.88–702231.6	5:24:31.88	−70:22:31.6	20.23	19.76	0.863	lmc163.6.26109	QSO-Aa	MgII, [OII]	Y	...	Y	...
MQS J052444.07–702601.9	5:24:44.07	−70:26:01.9	20.11	19.47	0.995	lmc163.7.63239	QSO-Aa	MgII, [OII]	Y
MQS J052502.45–705023.0	5:25:02.45	−70:50:23.0	20.08	19.38	1.333	lmc164.5.15592	QSO-Ba	CIII], MgII	Y	Y	Y	...
MQS J052521.42–710932.2	5:25:21.42	−71:09:32.2	20.11	19.13	1.410	lmc164.7.18253	QSO-Ba	CIII], MgII	Y	...	Y	...
MQS J052528.91–700448.6	5:25:28.91	−70:04:48.6	99.99	19.11	2.370	lmc162.8.45938	QSO-Aa	Ly α , CIV, CIII]	Y	Y	Y	...
MQS J052529.65–701018.9	5:25:29.65	−70:10:18.9	19.84	19.19	2.418	lmc163.5.109812	...	Ly α , SiIV, CIV	Y	...
MQS J052531.44–715356.0	5:25:31.44	−71:53:56.0	21.67	20.26	0.337	lmc165.8.14910	QSO-Aa	[OIII], H α	Y	...
MQS J052602.94–691638.1	5:26:02.94	−69:16:38.1	19.91	19.30	0.726	lmc161.2.53534	QSO-Aa	MgII, H β , [OIII]	Y
MQS J052612.77–695704.6	5:26:12.77	−69:57:04.6	19.96	19.25	1.690	lmc162.2.6599	QSO-Aa	CIV, CIII], MgII	Y	...	Y	...
MQS J052651.05–695809.5	5:26:51.05	−69:58:09.5	19.27	18.66	1.701	lmc162.2.22046	QSO-Aa	CIV, CIII], MgII	Y	Y	Y	...
MQS J052652.52–715322.7	5:26:52.52	−71:53:22.7	19.08	18.35	2.077	lmc165.1.705	QSO-Aa	Ly α , SiIV, CIV, CIII], MgII	Y	Y	Y	...
MQS J052705.98–702610.7	5:27:05.98	−70:26:10.7	99.99	20.75	1.390	lmc163.2.61689	QSO-Aa	CIII], MgII	Y
MQS J052745.27–700533.9	5:27:45.27	−70:05:33.9	18.68	18.02	1.249	lmc162.1.32008	QSO-Aa	CIII], MgII	Y	...	Y	...
MQS J052747.29–711058.9	5:27:47.29	−71:10:58.9	99.99	19.96	0.298	lmc164.1.26560	QSO-Aa	[OII], [OIII], H α	Y
MQS J052749.08–703641.7	5:27:49.08	−70:36:41.7	18.69	18.39	0.774	lmc163.1.57908	QSO-Aa	MgII	Y	Y	Y	...
MQS J052811.34–685651.5	5:28:11.34	−68:56:51.5	19.92	18.95	2.265	lmc161.4.71298	QSO-Aa	Ly α , SiIV, CIV, CIII]	Y
MQS J052855.60–693412.8	5:28:55.60	−69:34:12.8	20.56	19.51	0.293	lmc169.5.71795	QSO-Aa	[OIII], H α	Y
MQS J052908.79–702445.7	5:29:08.79	−70:24:45.7	19.75	18.89	2.020	lmc163.3.44161	QSO-Aa	SiIV, CIV, CIII], MgII	Y	...	Y	...
MQS J052925.45–695206.6	5:29:25.45	−69:52:06.6	20.83	19.15	0.291	lmc169.7.87162	...	[OIII], H α	...	Y
MQS J052931.17–702958.7	5:29:31.17	−70:29:58.7	20.12	19.63	0.682	lmc163.2.85221	QSO-Aa	MgII, H β , [OIII]	Y	Y
MQS J052943.61–693545.6	5:29:43.61	−69:35:45.6	20.31	19.72	0.440	lmc169.5.74380	QSO-Aa	MgII, [OII], H β , [OIII]	Y	...	Y	...
MQS J053018.98–694055.2	5:30:18.98	−69:40:55.2	99.99	20.81	0.417	lmc169.5.29449	QSO-Aa	[OII], [OIII]	Y
MQS J053044.94–712358.5	5:30:44.94	−71:23:58.5	19.87	18.90	1.340	lmc172.5.1149	QSO-Aa	CIII], MgII	Y	...	Y	YSO

TABLE 3 — *Continued*

Name	R.A.	Decl.	<i>V</i> (mag)	<i>I</i> (mag)	<i>z</i>	OGLE-III ID	KK09 Class	Emission Lines	Mid-IR	X-Ray	Var.	Notes
MQS J053120.33–715326.0	5:31:20.33	–71:53:26.0	19.35	18.34	1.359	lmc172.8.6749	QSO-Aa	CIII], MgII	Y	...	Y	...
MQS J053156.51–712031.0	5:31:56.51	–71:20:31.0	20.59	19.13	0.149	lmc172.5.41734	QSO-Aa	[OII], H β , [OIII], H α	Y	YSO
MQS J053159.70–712601.7	5:31:59.70	–71:26:01.7	19.14	18.37	1.217	lmc172.5.13874	...	CIII], MgII	Y	...
MQS J053225.83–713328.6	5:32:25.83	–71:33:28.6	21.99	20.72	0.647	lmc172.6.18567	QSO-Aa	[OII], H β , [OIII]	Y
MQS J053258.11–705112.9	5:32:58.11	–70:51:12.9	19.16	18.38	1.238	lmc171.5.30713	QSO-Aa	CIII], MgII	Y	Y	Y	YSO
MQS J053304.31–714848.4	5:33:04.31	–71:48:48.4	19.69	19.15	0.968	lmc172.8.43460	QSO-Aa	MgII, [OII]	Y	...	Y	...
MQS J053309.91–711149.7	5:33:09.91	–71:11:49.7	99.99	20.03	0.289	lmc171.8.45210	QSO-Aa	[OIII], H α	Y
MQS J053424.16–710748.2	5:34:24.16	–71:07:48.2	20.63	19.30	0.275	lmc171.2.8793	QSO-Aa	[OII], H β , [OIII], H α	Y	YSO
MQS J053536.04–712710.8	5:35:36.04	–71:27:10.8	19.41	18.62	1.799	lmc172.4.16498	QSO-Aa	CIV, CIII], MgII	Y	...	Y	...
MQS J053708.16–721747.5	5:37:08.16	–72:17:47.5	18.80	17.92	2.198	lmc180.7.609	QSO-Aa	Ly α , SiIV, CIV, CIII]	Y	...	Y	...
MQS J053741.18–715945.8	5:37:41.18	–71:59:45.8	19.62	18.85	1.386	lmc180.5.2714	QSO-Aa	CIII], MgII	Y	...	Y	...
MQS J053807.90–704847.8	5:38:07.90	–70:48:47.8	19.92	19.19	1.371	lmc178.5.10130	...	CIII], MgII	Y	...
MQS J054047.27–704828.9	5:40:47.27	–70:48:28.9	19.25	18.18	0.162	lmc178.4.531	QSO-Aa	H β , [OIII], H α	Y	Y	Y	...
MQS J054200.63–714011.4	5:42:00.63	–71:40:11.4	19.85	19.11	1.306	lmc179.2.21520	QSO-Aa	CIII], MgII	Y	...	Y	...
MQS J054227.27–720454.7	5:42:27.27	–72:04:54.7	99.99	21.19	0.415	lmc180.3.5664	QSO-Aa	[OIII]	Y
MQS J054258.91–713124.0	5:42:58.91	–71:31:24.0	22.00	20.21	0.263	lmc179.3.33404	QSO-Aa	[OIII], H α	Y	YSO
MQS J054319.60–715151.8	5:43:19.60	–71:51:51.8	21.52	20.10	0.584	lmc179.1.7700	QSO-Aa	[OII], H β , [OIII]	Y
MQS J054543.66–703957.1	5:45:43.66	–70:39:57.1	19.37	18.78	3.16	lmc185.8.35117	QSO-Aa	Ly α , SiIV, CIV	Y	...	Y	...
MQS J054639.57–712429.2	5:46:39.57	–71:24:29.2	20.85	19.74	0.262	lmc187.5.32609	QSO-Aa	H β , [OIII], H α	Y
MQS J054707.88–712244.9	5:47:07.88	–71:22:44.9	21.02	20.03	0.262	lmc187.5.36063	QSO-Ab	[OII], H $\gamma\delta\beta$, [OIII], H α	Y	YSO
MQS J054714.56–720850.4	5:47:14.56	–72:08:50.4	20.40	19.51	0.410	lmc188.6.13854	QSO-Aa	H β , [OIII]	Y
MQS J054739.69–712923.8	5:47:39.69	–71:29:23.8	19.69	18.11	0.209	lmc187.6.27610	QSO-Aa	[OII], [OIII]	Y
MQS J054758.68–720745.3	5:47:58.68	–72:07:45.3	19.28	18.79	0.793	lmc188.6.14068	...	MgII, [OII]	...	Y	Y	...
MQS J054822.47–713100.5	5:48:22.47	–71:31:00.5	19.87	18.48	0.211	lmc187.3.991	...	H β , [OIII], H α	...	Y	Y	...
MQS J054823.11–704543.9	5:48:23.11	–70:45:43.9	19.45	18.63	0.360	lmc186.4.32138	QSO-Aa	MgII, [OII], H $\delta\beta$, [OIII]	Y
MQS J054828.58–711246.4	5:48:28.58	–71:12:46.4	20.03	19.11	0.668	lmc186.1.21386	QSO-Aa	[OII], H β , [OIII]	Y	Y	Y	...
MQS J054853.69–722529.6	5:48:53.69	–72:25:29.6	19.90	19.39	0.942	lmc188.1.1376	QSO-Aa	MgII	Y
MQS J054917.21–713049.4	5:49:17.21	–71:30:49.4	20.44	18.99	0.190	lmc187.3.2954	QSO-Aa	[OIII], H α	Y
MQS J054950.04–710404.4	5:49:50.04	–71:04:04.4	19.82	19.27	0.719	lmc186.2.34388	QSO-Aa	MgII, [OII], H β , [OIII]	Y	Y	Y	...
MQS J055054.41–710038.4	5:50:54.41	–71:00:38.4	21.06	20.73	0.236	lmc186.3.21382	QSO-Aa	[OII], [OIII], H α	Y
MQS J055113.15–713339.7	5:51:13.15	–71:33:39.7	19.31	18.68	2.505	lmc187.3.22066	...	Ly α , SiIV, CIV, CIII]	...	Y	Y	...
MQS J055115.10–713629.5	5:51:15.10	–71:36:29.5	20.24	19.65	1.092	lmc187.3.24015	QSO-Aa	MgII	Y	...	Y	...
MQS J055135.06–713453.0	5:51:35.06	–71:34:53.0	18.87	17.92	1.387	lmc187.3.21276	QSO-Aa	CIII], MgII	Y	Y	Y	...
MQS J055148.48–715134.8	5:51:48.48	–71:51:34.8	20.12	18.65	0.215	lmc194.8.464	QSO-Aa	[OII], [OIII], H α	Y	YSO
MQS J055338.89–713751.5	5:53:38.89	–71:37:51.5	18.87	18.15	1.155	lmc194.7.6710	...	CIII], MgII	Y	...

NOTE. YSO—sources incorrectly classified as YSOs in Whitney et al. (2008), in 2MASS (Cutri et al. 2003), or in Gruendl & Chu (2009), HMXB—source incorrectly classified as a high mass X-ray binary in Sasaki et al. (2000).

TABLE 4
PARAMETERS OF 25 PREVIOUSLY KNOWN AGNs BEHIND THE LMC.

Name	R.A.	Decl.	<i>V</i> (mag)	<i>I</i> (mag)	<i>z</i>	OGLE-III ID	KK09 Class	Emission Lines	Mid-IR	X-Ray	Var	Notes
MQS J045356.54–694035.8	4:53:56.54	–69:40:35.8	19.04	18.09	0.279	lmc136.4.3318	QSO-Aa	H β , [OIII], H α	Y	...	Y	G
MQS J050846.00–700459.9	5:08:46.00	–70:04:59.9	19.88	19.24	1.175	lmc120.1.25861	QSO-Aa	CIII], MgII	Y	...	Y	G
MQS J051023.08–700735.5	5:10:23.08	–70:07:35.5	19.07	18.40	0.323	lmc112.8.10388	QSO-Aa	H β , [OIII], H α	Y	...	Y	G
MQS J051032.42–692715.8	5:10:32.42	–69:27:15.8	19.04	18.25	1.585	lmc111.8.45281	QSO-Aa	CIV, CIII], MgII	Y	...	Y	G
MQS J051259.55–703023.5	5:12:59.55	–70:30:23.5	19.63	19.00	1.299	lmc113.2.35781	QSO-Aa	CIII], MgII	Y	...	Y	G
MQS J051303.98–702250.4	5:13:03.98	–70:22:50.4	20.03	19.14	2.880	lmc113.3.9348	...	Ly α , SiIV, CIV, CIII]	Y	O
MQS J051412.14–702026.0	5:14:12.14	–70:20:26.0	18.57	17.94	2.323	lmc113.3.56510	QSO-Aa	Ly α , SiIV, CIV, CIII]	Y	...	Y	G
MQS J051433.46–693245.6	5:14:33.46	–69:32:45.6	18.55	17.78	1.344	lmc111.1.21832	QSO-Aa	CIII], MgII	Y	...	Y	D
MQS J051536.06–705401.2	5:15:36.06	–70:54:01.2	18.86	18.01	1.666	lmc114.3.18478	QSO-Aa	CIV, CIII], MgII	Y	...	Y	G
MQS J051626.32–694819.2	5:16:26.32	–69:48:19.2	18.47	17.88	0.626	lmc103.6.869	QSO-Aa	MgII, [OII], H β , [OIII]	Y	Y	Y	G
MQS J051628.84–683702.4	5:16:28.84	–68:37:02.4	17.29	16.74	0.455	lmc101.6.240	YSO-Aa	MgII, [OII], H $\delta\gamma\beta$, [OIII]	Y	Y	Y	G
MQS J051716.95–704402.0	5:17:16.95	–70:44:02.0	18.96	18.25	0.169	lmc104.8.13719	QSO-Aa	[OII], H $\delta\gamma\beta$, [OIII], H α	Y	...	Y	G
MQS J052056.97–702452.7	5:20:56.97	–70:24:52.7	18.21	17.62	1.815	lmc104.3.18078	QSO-Aa	CIV, CIII], MgII	Y	...	Y	G
MQS J052141.62–703028.9	5:21:41.62	–70:30:28.9	19.18	18.56	1.148	lmc104.2.17651	QSO-Ba	CIII], MgII	Y	...	Y	D
MQS J052247.19–710130.7	5:22:47.19	–71:01:30.7	19.44	18.57	1.719	lmc164.7.23460	QSO-Aa	CIV, CIII]	Y	...	Y	G
MQS J052247.69–704734.8	5:22:47.69	–70:47:34.8	18.98	18.20	1.641	lmc164.5.27868	QSO-Aa	CIV, CIII], MgII	Y	...	Y	G
MQS J052402.28–701108.7	5:24:02.28	–70:11:08.7	18.27	17.23	0.151	lmc163.5.76046	YSO-Aa	[OII], H $\delta\gamma\beta$, [OIII], H α	Y	...	Y	S1
MQS J053131.61–712947.0	5:31:31.61	–71:29:47.0	19.26	18.09	0.221	lmc172.6.34320	QSO-Aa	H $\delta\gamma\beta$, [OIII], H α	Y	Y	Y	E
MQS J053600.48–704127.7	5:36:00.48	–70:41:27.7	19.41	18.43	0.329	lmc170.1.28896	...	[OII], H β , [OIII], H α	...	Y	Y	G
MQS J055031.03–710957.1	5:50:31.03	–71:09:57.1	19.65	19.24	0.442	lmc186.2.17417	QSO-Aa	H β , [OIII]	Y	Y	Y	S2
MQS J050017.4–693215.9	5:00:17.39	–69:32:15.9	18.63	18.01	0.899	lmc128.4.38477	QSO-Aa	MgII	Y	...	Y	G
MQS J051140.7–710032.8	5:11:40.68	–71:00:32.8	20.06	19.24	1.560	lmc114.6.18703	QSO-Aa	CIV, CIII], MgII	Y	...	Y	G
MQS J051522.8–705806.2	5:15:22.84	–70:58:06.2	18.92	18.35	1.147	lmc114.3.18200	QSO-Aa	MgII	Y	...	Y	G
MQS J051853.1–690217.6	5:18:53.09	–69:02:17.6	20.16	19.37	1.620	lmc100.5.54060	QSO-Ba	CIV, CIII], MgII	Y	D
MQS J052716.2–693933.9	5:27:16.15	–69:39:33.9	19.48	19.16	0.845	lmc162.4.25325	QSO-Aa	MgII	Y	Y	Y	G

NOTE. — G-quasar discovered by Geha et al. (2003), O-QSO outburst from Clocchiatti et al. (2003), D-quasar discovered by Dobrzycki et al. (2002) or Dobrzycki et al. (2005), and S1–Seyfert Type 1 from Schmidtke et al. (1994), S2–Seyfert galaxy from Crampton et al. (1997), E–emission line galaxy.

TABLE 5
PARAMETERS OF THE REMAINING 677 TARGETED SOURCES.

Name	R.A.	Decl.	<i>V</i> (mag)	<i>I</i> (mag)	OGLE-III ID	Our spectral classification	SIMBAD match
MQS J044837.48–703619.0	4:48:37.48	–70:36:19.0	99.999	21.357	lmc137.8.7944	N	0
MQS J045155.55–703703.4	4:51:55.55	–70:37:03.4	19.678	18.813	lmc137.1.1081	red	0
MQS J045314.76–695918.0	4:53:14.76	–69:59:18.0	21.160	19.802	lmc136.2.4119	YSO/PN	0
MQS J045336.12–703502.2	4:53:36.12	–70:35:02.2	99.999	21.078	lmc137.2.24148	YSO	0
MQS J045339.37–703242.7	4:53:39.37	–70:32:42.7	20.578	20.128	lmc137.2.16965	N	YSO
MQS J045500.22–704619.7	4:55:00.22	–70:46:19.7	17.369	17.402	lmc130.5.303	Be	0
MQS J045723.01–710601.6	4:57:23.01	–71:06:01.6	99.999	20.957	lmc130.7.20197	N	Gal
MQS J045733.56–705808.4	4:57:33.56	–70:58:08.4	17.979	17.969	lmc130.6.15134	blue	0
MQS J050718.81–711332.3	5:07:18.81	–71:13:32.3	21.209	19.566	lmc122.1.15916	YSO	YSO
MQS J051702.46–690716.4	5:17:02.46	–69:07:16.4	99.999	18.358	lmc100.6.87292	PN	PN

NOTE. — We classified the remaining spectra into YSOs, PNe, Be stars, blue stars, and red objects, while other/featureless spectra are marked with an “N”. We also matched these objects to SIMBAD and give its classification with “0” meaning no match. (This table is available in its entirety in a machine-readable form in the online journal. A portion is shown here for guidance regarding its form and content.)